J. Electrochem. Sci. Eng. **16** (2026) 3224; https://doi.org/10.5599/jese.3224

Open Access : : ISSN 1847-9286
https://pub.iapchem.org/ojs/index.php/JESE

Original scientific paper

Integrated *in situ* RGB colorimetry and redox potential monitoring as a strategy for controlled synthesis of platinum nanostructures

Vladimir Guterman[1,2,✉], Kirill Paperzh[1,2], Elvira Zaitseva[1,3], Alina Khudoley[1], Elena Vetrova[4], Alina Nevelskaya[1,3], Anatoly Metelitsa[4], Ilya Pankov[4], Maria Danilenko[1] and Alexey Nikulin[1,3]

[1]*Faculty of Chemistry, Southern Federal University, 7 Zorge St., Rostov-on-Don 344090, Russia*
[2]*Prometheus R&D LLC, 4g/36 Zhmaylova St., Rostov-on-Don 344091, Russia*
[3]*Federal Research Center "The Southern Scientific Center of the Russian Academy of Sciences" (SSC RAS), Federal State Budgetary Institution of Science, 41 Chekhova St., Rostov-on-Don 344006, Russia*
[4]*Research Institute of Physical Organic Chemistry, Southern Federal University, 194/2 Stachki St., Rostov-on-Don 344090, Russia*

Corresponding Authors: ✉guter@sfedu.ru

Received: January 5, 2026; Accepted: March 7, 2026; Published: March 17, 2026

Abstract

Controlling the kinetics of liquid-phase synthesis is essential for elucidating transformation mechanisms and for tailoring the properties of precious metal nanoparticles (NPs) and nanostructured materials. This study examines the formation kinetics of Pt NPs and supported Pt/C materials via the reduction of H_2PtCl_6 using formic (FA), citric (CA), and ascorbic (AA) acids. It also analyses the structural, morphological, and electrochemical properties of the resulting materials. A key innovation is the validation of a novel approach that complements standard methods by combining RGB colorimetry with in-situ monitoring of the reaction medium's redox potential, specifically, open-circuit potential. This inexpensive technique provides data with accuracy and reliability comparable to established methods such as UV-vis spectroscopy, etc. The research identified distinct kinetic features of the Pt(IV) → Pt(0) transformation for each acid. Significant kinetic differences were observed, with NPs formation time decreasing in the order: FA > CA >> AA. Conversely, the electrochemically active surface area and catalytic activity for oxygen electroreduction increased in the order: AA << FA < CA. Owing to their superior structural characteristics, the Pt/C materials synthesized with citric acid demonstrated a higher electrochemical surface area and greater activity than a conventional commercial catalyst.

Keywords
Platinum nanoparticles; platinum-carbon nanocomposite; liquid phase synthesis; carboxylic acids effects; colouring changes; open circuit potential measurements; oxygen reduction reaction

Introduction

Nanoparticles (NPs) of precious metals and their alloys are increasingly being used in various fields of human activity [1-3]. Changes in the shape, size, and composition (in the event of alloys) of those NPs may have a significant effect on their properties and functional characteristics [1-5]. Therefore, in recent studies concerned with clarifying the relationship between the NPs nature/ /composition/structure and properties, focus has increasingly been given to the possibility of controlling the processes of their self-assembly [5,6].

It is even more difficult to control the properties of nanostructured materials containing NPs deposited on the surface of various dispersed supports. In addition to the properties of the NPs themselves and their size and structural characteristics, in this regard, an important role is played by the properties of the support material, as well as the conditions for applying metal NPs to the surface of that support.

A wide range of physical, chemical, and biological methods can be used to produce NPs of precious metals [1]. At the same time, the chemical reduction of metal precursors in the liquid phase remains the most popular and widespread method both in laboratory and, apparently, commercial practice [7-9]. Its advantages are determined by ease of use and energy efficiency, as well as by the presence of numerous factors that may influence the size and structure of NPs [8,10].

The range of methods used to study the processes of formation, growth, and (possible) aggregation of metal NPs in the liquid phase is quite wide [11-14]. Nevertheless, no experimental method can currently give a complete view of the complex processes involved in the nucleation and growth of NPs [11-14]. Most of these research methods cannot be used *in situ* in the process of NPs synthesis, and those that can be used in this way, *e.g*., ultraviolet-visible (UV-vis) spectroscopy, liquid-phase transmission electron microscopy (LP-TEM), X-ray powder diffraction (XRD), extended X-ray absorption fine structure (EXAFS) and X-ray absorption near edge structure (XANES) spectroscopy, small- and wide-angle X-ray scattering (SAXS/WAXS), and some others, require special high-cost devices and installations, such as a synchrotron, and special observation conditions, *e.g*. dilute solutions [11-14]. The use of these methods to study the kinetics and mechanism of the formation of deposited nanocomposites is further challenged. It is also obvious that most research methods cannot be used to study or control the kinetics of synthesis processes in real time under technological conditions when the concentrations of reagents in the liquid phase are high and the reaction medium is intensively stirred and subjected to gas purging. All this contributes to the liquid-phase synthesis being in a so-called “black box” state, *i.e.* although we may be aware of what is loaded into the reactor at the beginning and what is extracted at the end, it is not yet clear how the first turns into the second. Therefore, an urgent task for researchers in the development of optimal conditions for liquid-phase synthesis is to transition from the trial-and-error method to an approach that combines fundamental knowledge of the mechanisms of ongoing transformations with technologies that enable evaluation of changes in the state of the reaction medium during synthesis.

It is known that the reduction of precious metal precursors to NPs under conditions of liquid-phase synthesis is implemented through redox reactions, where formation of colloidal solutions of NPs is accompanied by a change in the colouring and/or transparency of the reaction medium [4,15,16]. In our recently published paper [17], we have implemented a new approach to study the kinetics of

liquid-phase synthesis for platinum NPs. It is based on a combination of two methods: i) continuous measurement of the intensity of three colouring components of the solution and ii) measurement of the indicator electrode potential, *i.e.,* the redox potential of the reaction medium, which changes over time. The simplicity of the proposed approach is combined with its applicability in technological environments and conditions, which, to a certain extent, compensates for the non-selectivity of the measured indicators. The fact is that both the solution colouring and the reaction medium redox potential, the values of which can also be measured during synthesis in suspensions, provide no accurate data on the nature or concentration of specific reagents.

While smartphone-based digital colorimetry has attracted significant interest due to its cost-effectiveness and portability, its application to non-plasmonic systems such as platinum remains under-developed [18]. Consequently, a significant gap exists in the scientific literature regarding a validated and comprehensive methodology for applying RGB colorimetry to the real-time kinetic analysis of Pt NPs formation. Subsequently, we detail an experimental setup with controlled illumination and measurement geometry (Figure S1, Supplementary material), which minimizes artifacts and enhances measurement reproducibility. This inexpensive, accessible, and robust method for kinetic analysis, using ubiquitous technology, enables broader research access, making it previously limited to those with access to expensive equipment. This approach will enable the real-time, high-throughput screening of synthesis conditions for noble metal nanoparticles and their alloys, accelerating the optimization of synthesis parameters for materials used, notably, as catalysts and sensors.

The choice of platinum as a research object for studying the nucleation/growth processes of metal NPs is due to both a lack of knowledge about the patterns of this metal NPs formation and a wide scope of application of platinum NPs in free form, or as part of nanocomposites [16,19]. In addition, the high catalytic activity of platinum in the reactions of electroreduction and electrooxidation, respectively, of oxygen (ORR) and hydrogen (HOR), allows us to obtain additional data on the characteristics of NPs and deposited platinum-carbon catalysts obtained as a result of those syntheses.

Thus, this study investigates a combined monitoring approach based on RGB colorimetry and redox potential measurement of the liquid-phase synthesis process as a simple and informative analytical method for studying the kinetics of Pt NPs formation. We compare data obtained under the conditions of liquid-phase synthesis of Pt NPs and platinum-carbon materials in aqueous-ethylene glycol solutions, where carboxylic acids - formic, citric, and ascorbic - act as reducing agents. These reducing agents have previously been used to produce platinum nanoparticles [5,15,20-23], and the reduction processes occur within a similar pH range, which enables testing the methodology specifically for elucidating the role of the reducing agent's nature in the kinetics of the multistage Pt(IV) → $Pt(0)_x$ transformation.

The work sets the following goals:

1. to assess the possibilities of using the approach proposed, including its informativeness and reliability, for studying the kinetics of the multistage reaction of transformation of $[PtCl_6]^{2-}$ into $Pt(0)_x$ NPs;
2. to study the effect of the nature of the reducing agent in a number of the above carboxylic acids on the kinetics of the transformation of $[PtCl_6]^{2-}$ into $Pt(0)_x$ NPs;
3. to compare the size and size distribution of platinum NPs formed in the course of the selected synthesis methods, finding out the role of the nature of the reducing agent in the structural and morphological characteristics of NPs;

4. to study the effect of a dispersed carbon support in the event of its introduction into the reaction medium before the synthesis on the kinetics of platinum reduction and the structural and morphological characteristics of the deposited Pt/C materials;
5. to study the electrochemical behaviour of the synthesized Pt/C materials, assessing the prospects of their use as the catalysts for the ORR in proton-exchange membrane fuel cells (PEMFCs).

Experimental

Materials and reagents

The following chemicals and materials were used in the experimental work: carbon support Vulcan XC72 (Cabot Corporation), ethylene glycol (extra pure, not less than 99.8 %, Rehacor, LLC), $H_2PtCl_6 \cdot 6H_2O$ (TU 2612-034-00205067-2003, mass fraction of Pt 37.6 %, Aurat, Russia), ascorbic acid (JSC Vekton, Russia), formic acid (JSC Vekton, Russia), citric acid (JSC Vekton, Russia), distilled H_2O (conductivity < 5 μS/cm, GOST 58144-2018), perchloric acid $HClO_4$ (extra pure, Sigma-Aldrich), Ar (99.9 %, Globus, Russia), 10 % aqueous Nafion® solution D1020, O_2 (from electrolyzer).

Methods and conditions to synthesize Pt NPs and produce Pt/C materials

The synthesis of Pt NPs was carried out in aqueous ethylene glycol (EG) solutions using ascorbic, formic, or citric acid as reducing agents. For this purpose, 3.95 mM of one of the acids was dissolved in a 250 mL chemical reactor containing 100 mL of an aqueous ethylene glycol solution with a component ratio of 55 % (H_2O) to 45 % (EG) by volume. The resulting reaction mixture was heated under constant stirring at 400 rpm to a set temperature (from 60 to 90 °C). After reaching the set temperature, the reaction mixture was purged with Ar for 30 min. Then, without stopping the argon purge, 20 mL of an aqueous 0.035 M solution of H_2PtCl_6 was introduced into the reactor with stirring. After the reaction was completed, the heating was ceased and the mixture was cooled naturally for 1 h with stirring. The Vulcan XC72 carbon support was then added to the colloidal solution of platinum NPs in the amount necessary to obtain the Pt/C material with a platinum mass fraction of 42 wt.%. The resulting suspension was stirred for 12 h for more efficient deposition of platinum NPs onto the support. The product was then filtered through a Büchner funnel using ashless filters, and the precipitate was repeatedly rinsed with isopropanol and bi-distilled water. The resulting Pt/C material was dried in a drying cabinet at 60 ℃ and then in a desiccator over P_2O_5 for 24 h.

The Pt/C materials in the carbon suspension were synthesized as described above, but the carbon support was introduced into the reaction medium before the synthesis. For this purpose, the suspension of the Vulcan XC72 carbon support was dispersed in ethylene glycol and mixed with an aqueous solution of the corresponding carboxylic acid. The subsequent synthesis, filtration, and drying of the material were carried out as described above.

The designation of the Pt/C materials corresponds to the synthesis method and conditions. For example, in the AA70, FA70, CA70, CA60, CA80, CA90, *etc*. designations, the letter part indicates a reducing agent used in the synthesis: AA - ascorbic acid, FA - formic acid, and CA - citric acid, and the numbers indicate the synthesis temperature: 60 to 90 °C.

Methods for studying the kinetics of transformation of Pt(IV) into $Pt(0)_X$

Control over changes in the colouring components of the reaction medium

During the Pt(IV) reduction, which led to the formation of a colloidal solution of platinum NPs in an aqueous ethylene glycol mixture, the colouring of the reaction medium changed from light yellow to

black (Figure S2). The colour change is due to the reduction of Pt(IV) ions (light yellow solution colour) to $Pt(0)_X$ NPs (black colour of the colloidal solution). The Celestron Handheld Digital USB Microscope Deluxe digital microscope was used to record the solution colouring during synthesis. To quantify the solution colouring intensity, we used a software developed by us that converts the colouring of the solution into three components of the additive RGB colour model [24], in which each shade of the continuously recorded image was determined by the contributions of three primary colours: red, green, and blue. This made it possible to graphically interpret the processes proceeding in the reaction medium, displaying a change in the quantitative content of each component over time.

To standardize the measurement process, all components of the setup were installed at specific positions (Figure S1). The same chemical reactor and the same volume of solution were used. The solution was illuminated during synthesis by a light source built into the digital microscope, set to maximum power. The influence of external lighting on the measurement result was very small; however, we maintained a standard state of external lighting. Figure S3 demonstrates the reproducibility of measurements of solution colour change over time.

Spectral studies were performed using the equipment provided by the Shared Use Center "Molecular Spectroscopy" of the Southern Federal University. The electronic absorption spectra of the reaction media were recorded using the Cary 50 spectrophotometer (Varian, USA) in the wavelength range from 220 to 800 nm.

The initial components of the synthesis, such as Pt(IV) and ascorbic acid, as well as the product of the Pt(IV) reduction reaction, show electronic absorption spectra in the UV region: the maximum absorption band of Pt(IV) is observed at a wavelength of 261 nm, for ascorbic acid, at a wavelength of 243 nm. At the same time, all the initial components exhibit zero absorption in the studied solutions at wavelengths longer than 420 nm. Therefore, we attributed any changes in absorption at 420 nm to platinum nanoparticles in solution, as was done earlier in [15]. The studied particles exhibit structureless absorption across the entire spectral range due to light scattering. As the concentration of NPs in the colloidal solution increases during the synthesis, the absorption at 420 nm increases.

The studies were performed in reaction media containing 0.058 mmol/L H_2PtCl_6. The working solutions were diluted with deionized water. The reference sample was a cuvette containing a reaction mixture without H_2PtCl_6. In the synthesis with ascorbic acid, the latter was also not added to the reference cuvette. The studies were performed using the UV-Cuvett Macro single-use cuvettes (optical path 10 mm).

Control over changes in the potential of the indicator electrode

In the course of synthesis, we measured the potential of the platinum indicator electrode immersed in the reaction medium (Figure S1). For this purpose, the reactor was equipped with a salt bridge, one tube of which was lowered into the reaction mixture and filled with it (before adding the chloroplatinic acid solution). The second tube was filled with a 3.5 M potassium chloride solution and lowered into a beaker with a solution of the same composition in which the silver/silver chloride electrode (reference electrode) was located. The electrodes were connected to the P-40X potentiostat (Elins LTD, Russia), which was used to record the potential difference between them, identical to the redox potential of the medium. The values of the potentials on the potentiometric curves measured during synthesis are given in the work relative to the standard hydrogen electrode (SHE). Figure S4 demonstrates the reproducibility of the results of measurements of the potential of the platinum indicator electrode.

Methods for studying the Pt/C materials composition and microstructure

Determination of platinum content in the Pt/C materials

The Pt content in Pt/C electrocatalysts was determined by thermogravimetry. Porcelain crucibles were calcined to constant mass at 800 °C, cooled and weighed. A ~0.02 g sample was heated in the crucible at 800 °C for 45 min. The Pt mass fraction was calculated from the mass difference between the pre- and post-combustion states. The error margin was ±1 %.

X-ray powder diffraction analysis

Structural analysis of the Pt/C catalyst was carried out using X-ray powder diffraction (XRD). Diffraction patterns were obtained at room temperature on an ARL X'TRA diffractometer (Bragg-Brentano geometry, CuKα radiation, λ = 0.154056 nm) over a 2θ range of 20 to 55° with a step size of 0.02°. Data processing was performed using SciDavis software to accurately determine peak parameters, particularly in cases of overlapping reflections arising from small crystallite sizes. This enabled refinement of the average size of coherent scattering regions (d_{Cr}). d_{Cr} was calculated using the Scherrer formula, as described in [25-27]. The estimated error margin was ±8 %.

Transmission electron microscopy

The size (d_{NPs}) and distribution of Pt NPs were examined using transmission electron microscopy (TEM) on a JEOL JEM-F200 microscope operating at 200 kV, the cold field emission gun with a current of 12 to 15 µA, the double-tilt Be specimen holder JEOL EM-01361RSTHB, and the CMOS AMT camera. For sample preparation, 0.5 mg of catalyst was dispersed in 1 mL of isopropanol via ultrasonication for 10 minutes. A drop of the suspension was placed on a copper grid coated with amorphous carbon (5 to 6 nm thick) and air-dried for 60 minutes. Size distribution histograms were constructed from measurements of at least 400 randomly selected particles across different sample regions. The error margin was ±0.2 nm.

Electrochemical methods

The electrochemical properties of the synthesized Pt/C materials were analysed using the rotating disk electrode (RDE) method. A catalytic layer was deposited on the glassy carbon electrode tip by preparing an ink composed of 0.0040 g of the catalyst, 200 µL of deionized water, 20 µL of Nafion (5 % solution) and 1.8 mL of isopropanol. This mixture was ultrasonicated for 25 minutes at a temperature of below 20 °C. Then, 6 µL of the ink was applied to the electrode tip and dried at 23 °C under rotation, yielding a catalyst loading of 20 µg(Pt) cm^{-2}.

Measurements were conducted in a three-electrode cell using 0.1 M $HClO_4$ as the electrolyte. The working electrode was the prepared catalytic layer on the RDE tip, with a platinum wire as the counter electrode and a silver/silver chloride electrode (Ag/AgCl, 0.208 V) as the reference. A VersaSTAT3 (Ametek, USA) potentiostat was employed, and all potentials are referenced to the reversible hydrogen electrode (RHE).

Activation of the Pt/C surface and determination of the electrochemically active surface area

The Pt/C electrode surface was activated by 100 voltammetric cycles between 0.04-1.0 V (RHE) at 200 mV s^{-1} in Ar-saturated 0.1 M $HClO_4$. Subsequently, two cyclic voltammograms were recorded at 20 mV s^{-1} in the same range. The electrochemically active surface area (ESA) was determined from the second CV by integrating the charge associated with hydrogen monolayer adsorption and desorption, following the procedure outlined in [28]. The error margin was ±10 %.

Determination of the catalyst activity in the oxygen electroreduction reaction

To assess the catalytic activity toward the oxygen reduction reaction (ORR), the electrolyte (0.1 M $HClO_4$) was purged with O_2 for 1 hour at ambient pressure. Following activation, linear sweep voltammograms were obtained at rotation speeds of 400, 900, 1600 and 2500 rpm within a potential window of 0.1-1.1 V (RHE) at a scan rate of 20 mV s^{-1}. Kinetic currents at 0.90 V (RHE) were calculated *via* the Koutecký-Levich equation [29], accounting for mass transport limitations under RDE conditions. ORR performance was evaluated based on kinetic current normalized to the platinum mass (mass activity) or electrochemically active surface area (specific activity). The systematic error in the activity measurements was 10 %.

Results and discussion

Kinetics of Pt NPs formation followed by time changes in the colouring of solutions

The formation of metal NPs in solution, resulting from the chemical reduction of a metal compound, is a typical manifestation of a heterogeneous reaction that involves nucleation and particle growth. The formation of platinum NPs from Pt(IV) compounds is accompanied by a characteristic change in the colouring and transparency of the solution [30], *i.e*. a transparent light-yellow solution, the colour of which is caused by the presence of $[PtCl_6]^{2-}$ cations in the solution, darkens as the reaction proceeds and eventually turns into a dark opaque colloidal solution of platinum NPs (Figure S2). Initially, the change in the colouring is due to the transformation of Pt(IV) → Pt(II) [4]. The change in the composition of the coordination shell of Pt(IV) and Pt(II) ions may also have an effect on the colouring of the solution [4]. The subsequent formation of $Pt(0)_x$ solid-phase particles and changes in their shape and size also affect light scattering and adsorption. The formation of a colloidal solution of platinum NPs causes a decrease in the light transmittance and a change in the colouring of the reaction medium to black [31].

Following the introduction of chloroplatinic acid to aqueous ethylene glycol solutions of formic, citric, or ascorbic acids, all the chemical reactions proceed in a highly acidic medium. This further enhances the similarity of the colouring of all three solutions in the initial and final (after the formation of platinum NPs) states. At the same time, the duration of the colour transition, as well as some features of the intensity changes of the three colour components over time, differ significantly for each reducing agent (Figure 1).

We thus consider the general patterns and particular features characteristic of each specific reducing agent, as well as the peculiarities of a change in the intensity of the solution three colouring components (Figure 1). The key (most noticeable) stages in all the systems on the colouring-intensity versus time (ClrInt - *t*) curves are sharp, consistent changes in the intensity of all three colours of the platinum NP solution. In synthesis processes with three reducing agents, the greatest change in colour intensity during the formation of platinum NPs is observed for the blue component.

The time preceding an abrupt change in the solution colour during darkening can be considered the induction period of the nucleation process for particles of a new phase. The induction period decreases in the order FA70 > CA70 >> AA70. The achievement of a stationary and almost identical intensity of all three components of the solution colouring, which corresponds to the formation of a dark, almost opaque solution of platinum NPs, is accelerated in the same order. It is noteworthy that at the stage preceding an abrupt change in the solution colouring, the coordinated change in the intensity of the three colouring components is not monotonous, which is especially noticeable for the solutions of formic and citric acids (Figures 1a and 1b).

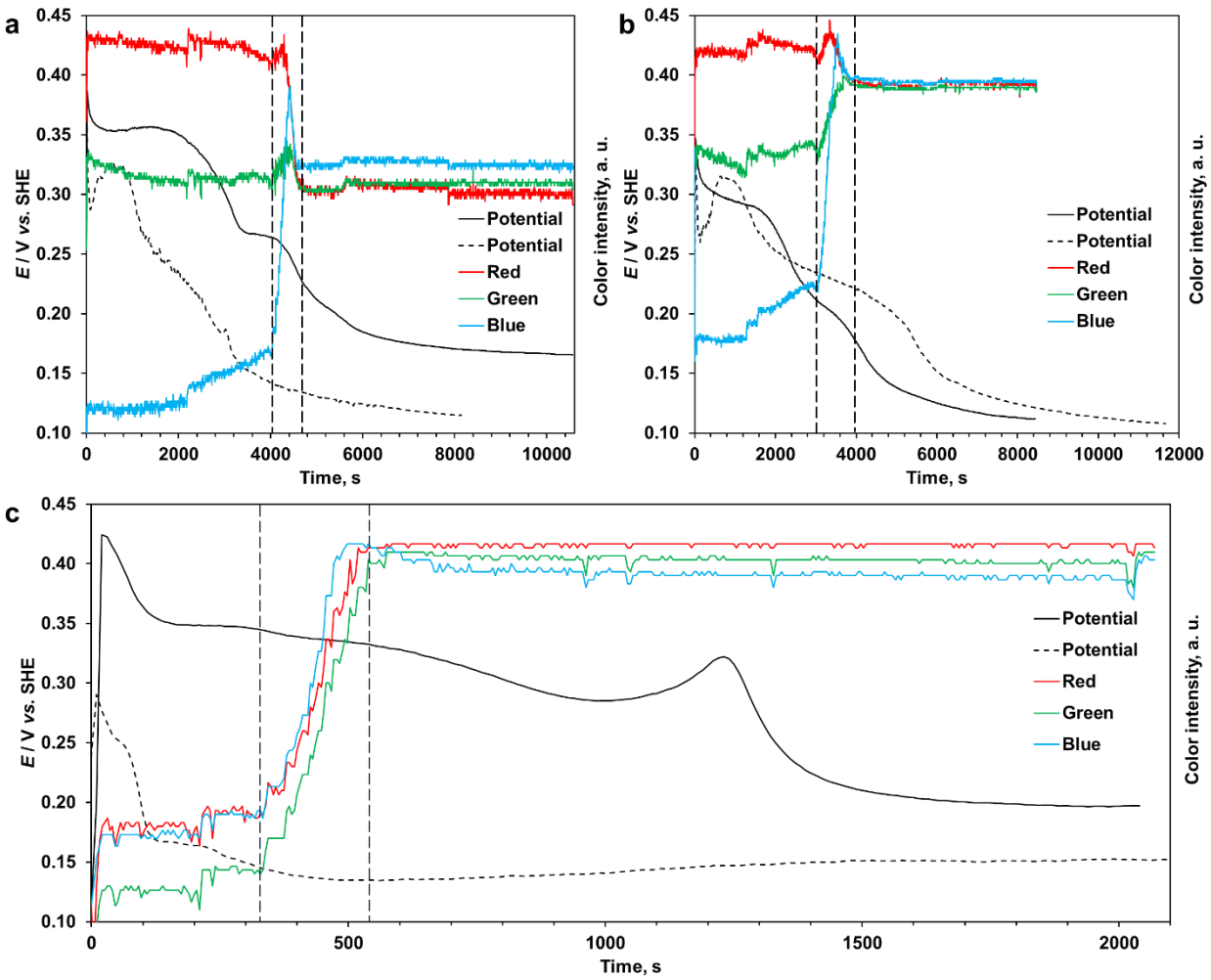

Figure 1. *Time changes in the three colouring components (coloured lines) and the reaction medium redox potential (black lines) during the synthesis of platinum NPs in the solution (solid line) and in the suspension (dotted line). Reducing agent: (a) formic acid, (b) citric acid and (c) ascorbic acid. The synthesis temperature: 70 °C, Ar atmosphere*

By non-monotonicity, we mean a regular stepwise change in colour, followed by periods of stationarity or monotonic increases or decreases in intensity (as observed for the blue component in Figures 1a to 1c), rather than frequent, minor intensity fluctuations associated with solution stirring and gas flushing. Such fluctuations in colour intensity can be associated with changes in pH and transformations in the forms in which platinum is present in solution; however, the specific composition of the compounds formed, as well as the causes of the transformations, remains unknown. Since all the studied transformations of Pt(IV) → Pt(0) proceed in aqueous ethylene glycol solutions, it is important to understand whether ethylene glycol may act as a co-reductant that has a significant effect on the kinetics of this multistage reaction. The study of the colour transition in an aqueous ethylene glycol mixture containing no carboxylic acids at 80 °C has shown that ethylene glycol does indeed reduce Pt(IV) to metal NPs. The stage of an abrupt change in the solution colouring intensity is observed in the time range of about 5,000 to 6,000 s from the moment of introducing H_2PtCl_6 (Figure S5), whereas in aqueous ethylene glycol media containing the studied carboxylic acids, even at a lower temperature (70 °C), the above occurs much earlier, *i.e.* in the time range of 4,000 to 4,300 s for the formic acid solution and even faster for other reducing agents (Figure 1). Taking into account the nature of the change in the reaction medium redox potential during synthesis (see below), we may consider carboxylic acids as the main reducing agents for

platinum precursors in the studied solutions, although this also suggests the possibility of a parallel, slower reduction of platinum precursors by ethylene glycol.

Analysis of ongoing transformations using UV-vis spectroscopy

To clarify the kinetics of the transformation of different forms of platinum and confirm the correct identification of the NPs nucleation/growth stage by an abrupt change in the intensity of the solution three colouring components, we have analysed the composition of the samples taken from the reaction mixtures at different synthesis stages using UV-vis spectroscopy. Figure 2 shows the absorption spectra for Pt(IV) and $Pt(0)_x$ NPs corresponding to different sampling moments. In Figure 3, the experimentally recorded dependences of the solution three colouring components and the medium redox potential on time are compared in the same time range, including the time dependencies of the solution absorption at wavelengths (λ) of 261 and 420 nm plotted according to the results of UV-vis spectroscopy (Figure 2). The solution absorption at λ = 261 nm is proportional to the concentration of Pt(IV), while at λ = 420 nm, to the concentration of platinum NPs in the colloidal solution. For the reaction medium samples taken during the ascorbic acid synthesis, it was not possible to record any Pt(IV) signal at λ = 261 nm due to the overlap of absorption spectra with ascorbic acid (λ = 243 nm). The signal intensity of ascorbic acid itself was thus measured at λ = 243 nm. In this case, it is important to consider that ascorbic acid is consumed for the reduction of both Pt(IV) and Pt(II).

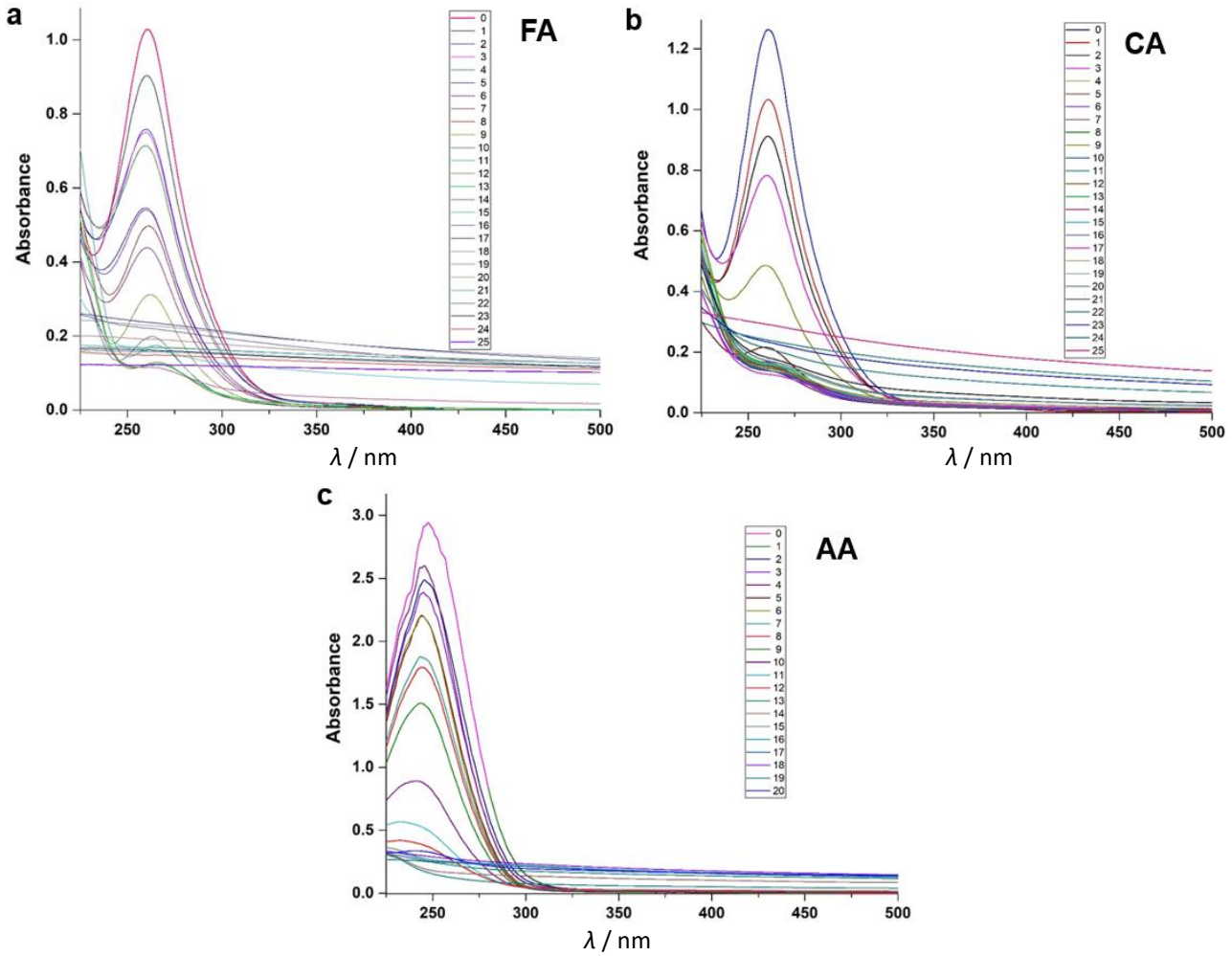

Figure 2. *Time-resolved UV-vis spectra for the Pt NPs formation. Reducing agent: (a) formic acid, (b) citric acid and (c) ascorbic acid. The numbering of the curves corresponds to the order of sampling of the reaction medium during synthesis (see the markers on the E - t curves in Figure 3)*

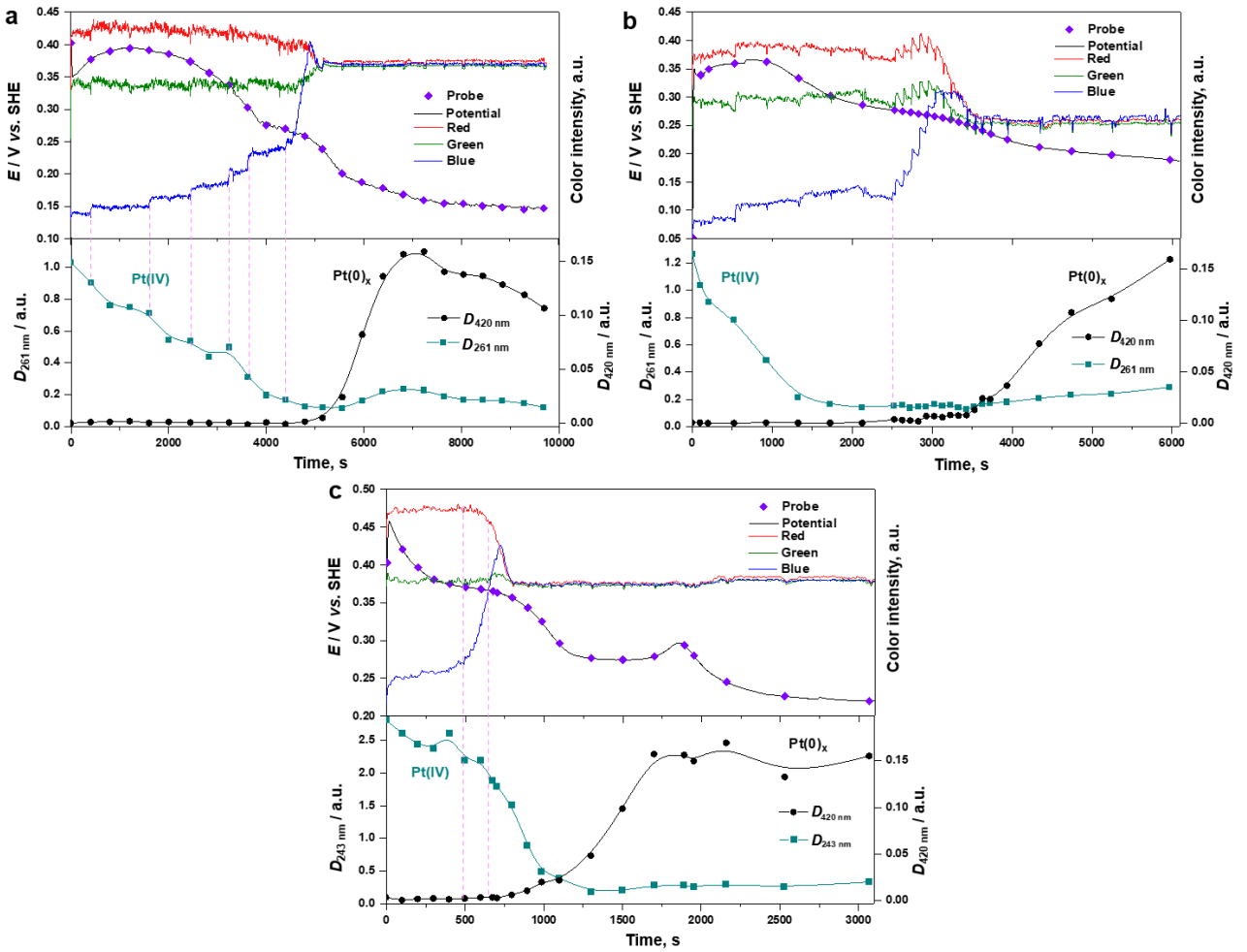

Figure 3. *Changes in the solutions three colouring components and the indicator electrode potential during synthesis (the upper part of each figure), as well as absorption of the solutions sampled during the Pt(IV) reduction (the lower part of each figure). The markers on the E - t curves correspond to the moments of sampling from the corresponding reaction mixture. Reducing agent: (a) formic acid, (b) citric acid and (c) ascorbic acid*

In all the syntheses, on the curves of changes in the absorption of the solutions prepared from the samples taken at different points in time, we may observe: i) a decrease and subsequent stabilization of the Pt(IV) absorption signal ($D_{261\ nm}$, formic and citric acid syntheses) or the ascorbic acid signal ($D_{243\ nm}$, ascorbic acid synthesis) and ii) the moment when a signal from platinum NPs appears ($D_{420\ nm}$), as well as the subsequent increase in its intensity (Figure 3). However, each synthesis has its own features in terms of the mutual correspondence of the ClrInt - *t* curves and changes in the intensity of the corresponding UV absorption spectra.

When reducing the platinum precursor with formic acid, the period of abrupt change in the solution colouring corresponds exactly to the moment of signal stabilization on the absorption curve for the Pt(IV) solution and the beginning of growth of the $Pt(0)_x$ signal (Figure 3a). The non-monotonic nature of the change in the concentration of Pt(IV) in the samples taken during synthesis generally correlates with a non-monotonic change in the solution colouring intensity. The moments of that change are indicated by vertical dotted lines in Figure 3a. At the same time, it is unlikely that the non-monotonic change in $D_{261\ nm}$ is associated with inaccuracies in sampling, since following the formation of platinum NPs, signal fluctuations at λ = 261 nm are no longer recorded. The increase and subsequent decrease of the $D_{420\ nm}$ associated with the formation of a colloidal solution of platinum NPs and their concentration in the solution (Figure 3a) may be due to secondary processes of nanoparticle aggregation.

In the event of the synthesis with citric acid, the decrease in the concentration of Pt(IV) (decrease in the $D_{261\ nm}$) is completed approximately 2,000 s after the beginning of the synthesis, and the appearance of a signal from platinum NPs ($D_{420\ nm}$) is recorded at the beginning of an abrupt increase in the colouring intensity of the solution, approximately in 2,500-3,000 s (Figure 3b, vertical dotted line). The signal intensity from ascorbic acid decreases due to its oxidation by Pt(IV) and Pt(II) compounds and stabilizes approximately 1,300 s after the beginning of the synthesis (Figure 3c).

The presence of platinum NPs in the selected samples (signal at λ = 420 nm) is recorded a little later than the beginning of an abrupt change in the intensity of the blue component of the reaction medium colouring (Figure 3c). Interestingly, in the ascorbic acid synthesis, the abrupt change in the intensity of the red and green colouring components begins somewhat later than for the blue component (see dotted segments in Figure 3a). It is worth noting that in the formic acid and ascorbic acid syntheses, the concentration of platinum NPs (signal intensity at λ = 420 nm) grows long after the stabilization of the three colouring components intensity on the ClrInt - *t* curves, only then stabilizes. In the event of the citric acid synthesis, the increase in the concentration of platinum NPs (signal intensity at λ = 420 nm) generally continues throughout the entire measurement period. Since the intensity of light absorption depends not only on the concentration of NPs in the colloidal solution but also on the NPs size [32]. It cannot be excluded that the observed signal growth at λ = 420 nm is associated with both an increase in NP concentration during the reaction and an increase in their size.

In general, we may draw a conclusion that the onset of an abrupt change in the colouring intensity measured during the synthesis on the ClrInt - *t* curves allows us to accurately record the moment of the beginning of the formation of platinum NPs in the reaction medium, although the increase in the NPs concentration in the solution and/or their growth continue after the stabilization of the solution colouring intensity on the ClrInt - *t* curves.

Kinetics of Pt NPs formation and Pt/C materials production followed by time changes in the medium redox potential

Another indicator of transformations occurring in the reaction medium during synthesis is the potential of the indicator electrode, which changes as the nature and concentration of oxidizing and reducing agents in the reaction mixture vary (Figures 1, 3 and S3-S7). The reaction vessel contains a platinum indicator electrode, whose potential reflects the solution composition, and an electrolytic junction connected to the Ag/AgCl reference electrode immersed in KCl solution. Thus, the potential of the indicator electrode, which changes during the synthesis, is measured relative to an electrode whose potential remains constant. The usefulness of the open-circuit potential (OCP) measurement technique for studying the nucleation and growth of platinum nanoparticles in the liquid phase is substantiated by research papers [33,34].

Since the reducing agent is taken in excess in all three synthesis processes, a greater influence on a change in the value of the medium redox potential should be exercised by a decrease in the concentration of oxidants, *i.e.,* successively converted forms of Pt(IV) and Pt(II). Indeed, despite the differences in the type of E-t curves across synthesis methods, the *E* value decreases as the oxidizer is consumed, with two consecutive potential delays observed on the curves. Taking into account the literature data [35], these may be associated with the transformations of Pt(IV) + 2ē → Pt(II), and Pt(II) + 2ē → Pt(0). It should be noted that on the potential decline curve, during the ascorbic acid synthesis, we may observe a reproducible local maximum at the second potential delay (Figures 1c, 3c, S4), the nature of which is unclear.

The *E-t* curves recorded during synthesis are similar to those of potentiometric titration, i.e., in both cases, the potential at each time point is determined by the nature and concentrations of the oxidized and reduced forms of each reagent involved or formed in the reaction. However, in redox potentiometric titration, rapidly reacting oxidizers and reducing agents are used, for which the compositions of the corresponding oxidized and reduced forms are well known. In the course of the platinum NPs liquid-phase synthesis, slow, multistage transformations of an oxidizer ($[PtCl_6]^{2-}$) and a reducing agent (carboxylic acid) proceed, as a result of which several intermediate oxidants and reducing agents can simultaneously be present in the solution, the concentration of which varies. This causes the complex nature of the potentiometric curves recorded during the synthesis of platinum NPs (Figures 1 and 2).

A comparison of the ClrInt - *t* and *E* - *t* curves shows that during the formic acid and citric acid syntheses, the nucleation stage of platinum NPs corresponds to the final part of the second delay and the beginning of the potential decline, namely, a section presumably associated with the following reaction: Pt(II) + $2e^-$ → Pt(0) (Figure 1a and 1b). On the Pt(II) potentiometric titration curves, a similar section might be called as preceding the equivalence point. A more complex picture emerges in the ascorbic acid synthesis. The moment of the beginning of the NPs nucleation corresponds to the final part of the first potential delay (Figures 1c and S6), whereas the process of reducing the platinum compounds and increasing the concentration of $Pt(0)_x$ NPs in the solution continues during the period corresponding to the second potential delay (Figure 3c). At the same time, a more precise examination of the *E* - *t* curve for the ascorbic acid synthesis shows that at the first potential delay, which we associate with the reduction of Pt(IV) to Pt(II), there is an inflection on the curve, indicating a more complex nature of the processes (Figure S6).

It should be noted that in all the syntheses, the decline of the redox potential before reaching a stationary value continues for quite a long time after the formation of the first platinum NPs (blackening of the solutions) (Figures 1 and 3). The correspondence of certain sections of the *E* - *t* curves to the stage of an abrupt change in the solution colouring on the ClrInt - *t* curves corresponding to the nucleation of NPs allows us to approximately determine the potential values at which nucleation begins (proceeds). The results of comparing the total duration of the Pt(IV) → $Pt(0)_x$ transformation, the induction period preceding an abrupt change in the solution colouring, the duration of the nucleation period (period of an abrupt change in the colouring of the solution), and the values of the NPs nucleation potentials are shown in Figure 4.

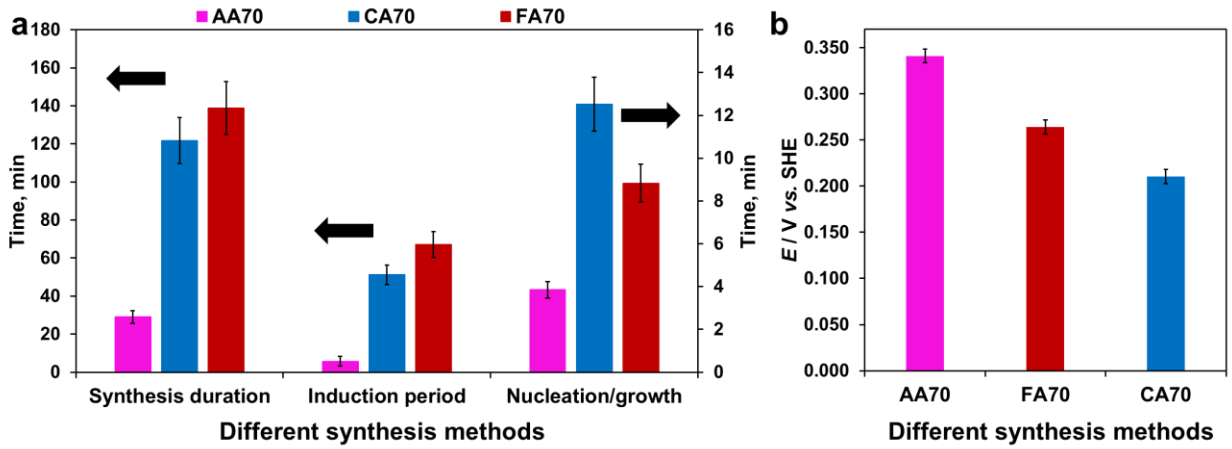

Figure 4. *(a) Duration of the induction period and the period of the NPs nucleation, as well as total synthesis duration for platinum NPs; (b) potential values of the platinum NPs nucleation onset for each synthesis method*

The nucleation of platinum NPs in the ascorbic acid synthesis begins at the highest redox potential, with all the reaction stages proceeding much faster than in the formic acid and citric acid syntheses, for which the duration of the corresponding stages is quite close (Figure 4). The platinum NPs nucleation onset potentials decrease in the order AA > FA > CA. At the same time, the difference between these potentials is not very large, with a range of 0.21-0.34 V (Figure 4b).

The ability to measure the redox potential of the reaction medium during syntheses in carbon suspensions has enabled evaluation of the effect of the support on reaction kinetics. The corresponding *E* - *t* curves are shown in Figure 1 with dotted lines. In the event of the citric acid synthesis, the duration of transformation in the suspension turns out to be slightly higher than in the solution of a similar composition (Figure 1b). On the *E* - *t* curves, we may observe potential delay areas, although the first delay is transformed into an extended maximum, as with formic acid (Figure 1a). On the *E* - *t* curve for the formic acid synthesis in the suspension, we may also observe a small local maximum in the area of completion of the second potential delay (Figure 1a). Nevertheless, there is no critical change in the general appearance of the *E* - *t* curves when using citric and formic acids as the reducing agents (Figure 1a and 1b). The introduction of dispersed carbon with high surface area into the initial mixture is believed to promote the sorption of part of the citric acid and to decrease its concentration in solution. As a result, the reduction reaction of platinum compounds, which begins after the introduction of H_2PtCl_6 to the reactor, proceeds more slowly in the liquid phase volume than in the solutions containing no carbon. The presence of a dynamic equilibrium between the dissolved and absorbed reducing agents should also influence the kinetics of interaction with the oxidizer.

A different situation is observed in the solutions of ascorbic acid (Figure 1c). The synthesis in the suspension proceeds much faster than in the solution, and the type of *E* - *t* dependence is changing significantly (Figure 1c). In addition, during the synthesis in the suspension, the local maximum characteristic of the synthesis in the solution disappears on the *E* - *t* curve. We believe that the acceleration of synthesis in a carbon suspension based on ascorbic acid solution is due to the significant contribution of the heterogeneous nucleation of platinum nanoparticles on the carbon surface, which occurs at a high rate. The disappearance of the local maximum on the *E* - *t* curve may be due to the sorption of intermediate ascorbic acid oxidation products by carbon, which prevents them from being adsorbed on the surface of the indicator electrode and from affecting its potential.

The solutions of formic acid (Figure 1a) are characterized by a slight acceleration of transformation into the suspensions compared to the solution. Perhaps, in this case, the precursor reduction rate is influenced by both the sorption of acid by carbon and the “connection” of heterogeneous nucleation to homogeneous one.

It is obvious that during the NPs nucleation and growth, as well as upon completion of their formation, the NPs aggregation processes in the colloidal NPs solution or in the corresponding carbon suspension, affect the microstructure of the resulting product. Measuring the intensity of the solution colouring components and the redox potential of the reaction medium cannot provide any information on these processes. At the same time, the fact that the redox potential reaches a stationary value, which is observed in all the studied systems, actually indicates the establishment of constant concentrations of the components involved in complex redox transformations, which is identical to the completion of the transformation of platinum compounds into metal NPs.

Composition and microstructure of the synthesized Pt/C materials

The platinum mass fraction in the synthesized Pt/C materials was quantified by gravimetric analysis (see Experimental section). It turns out to be close to the calculated one (42 wt.%) (Table 1).

It should be noted that in the materials obtained in the carbon suspension, the mass fraction of platinum increases slightly compared to the samples obtained by depositing the NP colloid onto a support (Table 1). This is most likely due to the rapid sorption of the formed NPs from the reaction medium by the carbon support. When the temperature is increased to 80 and 90 °C during the CA synthesis, the differences in the platinum mass fraction are within the margin of error. The Pt/C materials microstructure has been studied by X-ray powder diffraction and electron microscopy (see Experimental Section). The X-ray diffraction patterns for the synthesized Pt/C materials are shown in Figure 5, with the average crystallite sizes calculated from the half-width of the (111) platinum maximum shown in Table 1.

Table 1. *Composition and structural and morphological characteristics of the Pt/C materials*

Sample	Pt loading, wt.%	d_{Cr} / nm (XRD)	d_{NPs} / nm (TEM)
AA70_solution	36.8±0.4	3.0±0.3	–
AA70_suspension	40.6±0.4	4.6±0.5	3.2±0.3
FA70_solution	38.0±0.4	3.4±0.3	–
FA70_suspension	39.5±0.4	3.2±0.3	2.9±0.3
CA70_solution	40.9±0.4	2.9±0.3	–
CA70_suspension	40.2±0.4	2.3±0.2	2.7±0.3
CA60_solution	35.2±0.4	2.7±0.3	–
CA60_suspension	38.1±0.4	2.5±0.3	2.5±0.3
CA80_solution	40.0±0.4	2.7±0.3	–
CA80_suspension	39.2±0.4	2.2±0.2	2.4±0.2
CA90_solution	37.2±0.4	3.4±0.4	–
CA90_suspension	37.5±0.4	2.3±0.2	2.5±0.3

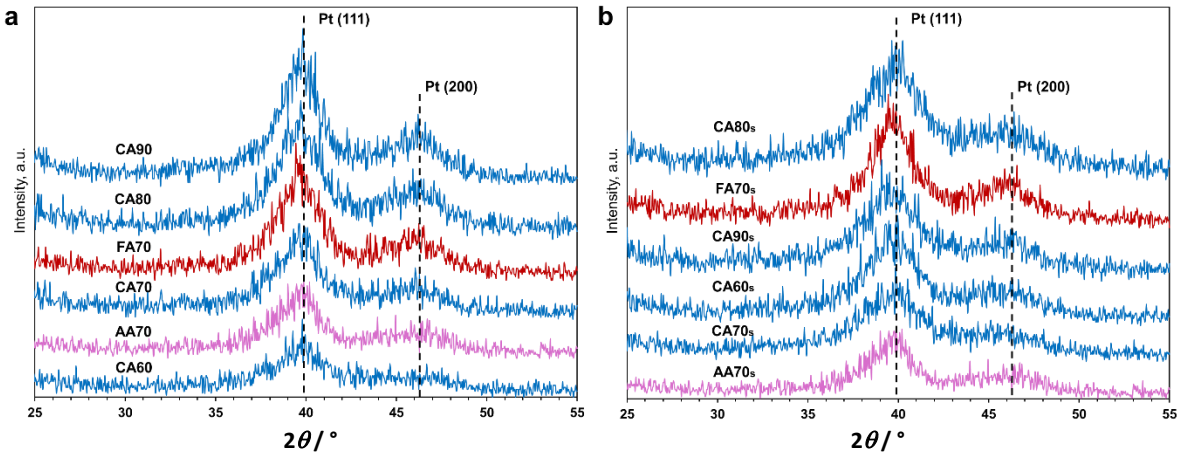

Figure 5. *X-ray diffraction patterns for the Pt/C materials obtained during the syntheses in (a) solutions and (b) carbon suspensions*

The characteristic <111> and <200> reflections of the platinum phase are broadened in all diffraction patterns measured due to the small crystallite size. The average size of crystallites decreases in the order AA70 >FA70 ≥ CA70 (Table 1). In the case of formic and citric acids, the size of platinum crystallites decreases during the transition from solution to suspension synthesis, whereas it increases for ascorbic acid synthesis (Table 1).

For the citric acid synthesis, which has resulted in obtaining crystallites of the smallest size, we have studied the effect of temperature on both the kinetics of NPs nucleation/growth and the size of crystallites. The ClrInt - *t* and *E* - *t* dependences measured for the syntheses at temperatures of 60, 70, 80 and 90 °C are shown in Figure S7. With increasing temperature, the formation of platinum NPs accelerates, as a result of which the length of both the ClrInt - *t* and *E* - *t* curves, as well as of

their characteristic sections, is reduced. The form of the corresponding dependencies is preserved, and the range of changes in the reaction medium redox potential remains the same. At the same time, the E-t dependences at 70 to 90 °C for suspension synthesis are slightly shifted toward higher potentials, apparently due to reduced citric acid concentration in the solution, resulting from partial sorption by the support. The potential values corresponding to the onset of platinum NP nucleation also do not depend on temperature within the measurement error. All these can be considered indirect confirmation of the preservation of the chemical mechanism of transformations occurring during citric acid synthesis in the temperature range of 60 to 90 °C. It should be noted that the acceleration of all stages of the synthesis of platinum NPs with increasing temperature leads to no significant change in the size of crystallites (Table 1).

Previously, we have observed a decrease in the average size of platinum crystallites during the transition from solution synthesis to suspension synthesis for two of the three synthesis methods studied. The enhancement of the Pt/C materials microstructure in the case of the citric acid synthesis in the suspension is also indicated by the authors in [36]. In consideration of the foregoing, we have studied the microstructure of the Pt/C materials synthesized in the suspensions by transmission electron microscopy (TEM) (Figure 6, Table 1). The average size of NPs in the studied materials is close to the crystallite size, decreasing in the same order (AA70 > FA70 ≥ CA70) from 3.2 to 2.55 ± 0.15 nm. The change in the temperature of the citric acid synthesis does not significantly affect the size of platinum NPs in the same manner as it has been recorded for crystallites. For the samples synthesized by the citric acid method at temperatures from 60 to 90 °C, both the average NP size and the histograms of their size distribution are nearly identical (Figure 6).

The histograms of the NPs' size distribution indicate the widest dispersion for the AA70 sample synthesized using ascorbic acid (Figure 6). Studying the micrographs of the AA70 sample indicates a significant difference in its morphology from the other materials, *i.e.* it is characterized by a predominant aggregation of NPs into “nanoflowers”, which causes a strong non-uniform distribution of NPs over the surface of the support (Figure 6a).

The aggregation of NPs into nanoflowers in the syntheses using ascorbic acid as the reducing agent has previously been established by the authors in [37,38]. It is obvious that the coalescence of NPs into such nanoflowers should lead to a significant decrease in the platinum electrochemically active surface area (ESA). The fusion of several crystallites within those aggregates is likely to yield a high average crystallite size, as determined from the XRD data. In this regard, the calculation of the average size of NPs can be carried out only for individual NPs, the number of which is relatively small in the micrographs of the AA70 sample. It is this feature that may be the reason for $d_{Cr} >> d_{NPs}$ for the AA70 sample (suspension) (Table 1).

The size of the critical nucleus during the electrodeposition of metals is inversely proportional to the third power of the overpotential and is directly proportional to the surface energy (σ_{surf}) [39]. In the event of the liquid-phase redox synthesis, an analog of overvoltage is the difference between the potential of the oxidizer (Pt(II) compounds) and the nucleation potential (Figure 3b), which grows slightly in the order AA70 < CA70 < FA70. Unfortunately, it is not possible to quantify the effect of the nature of carboxylic acids used as the reducing agents on the value of σ_{surf}.

At the same time, it is known that citric acid and its oxidation intermediates are quite effective surfactants that are easily adsorbed on the surface of growing platinum NPs and, thus, reduce the σ_{surf} value [40].

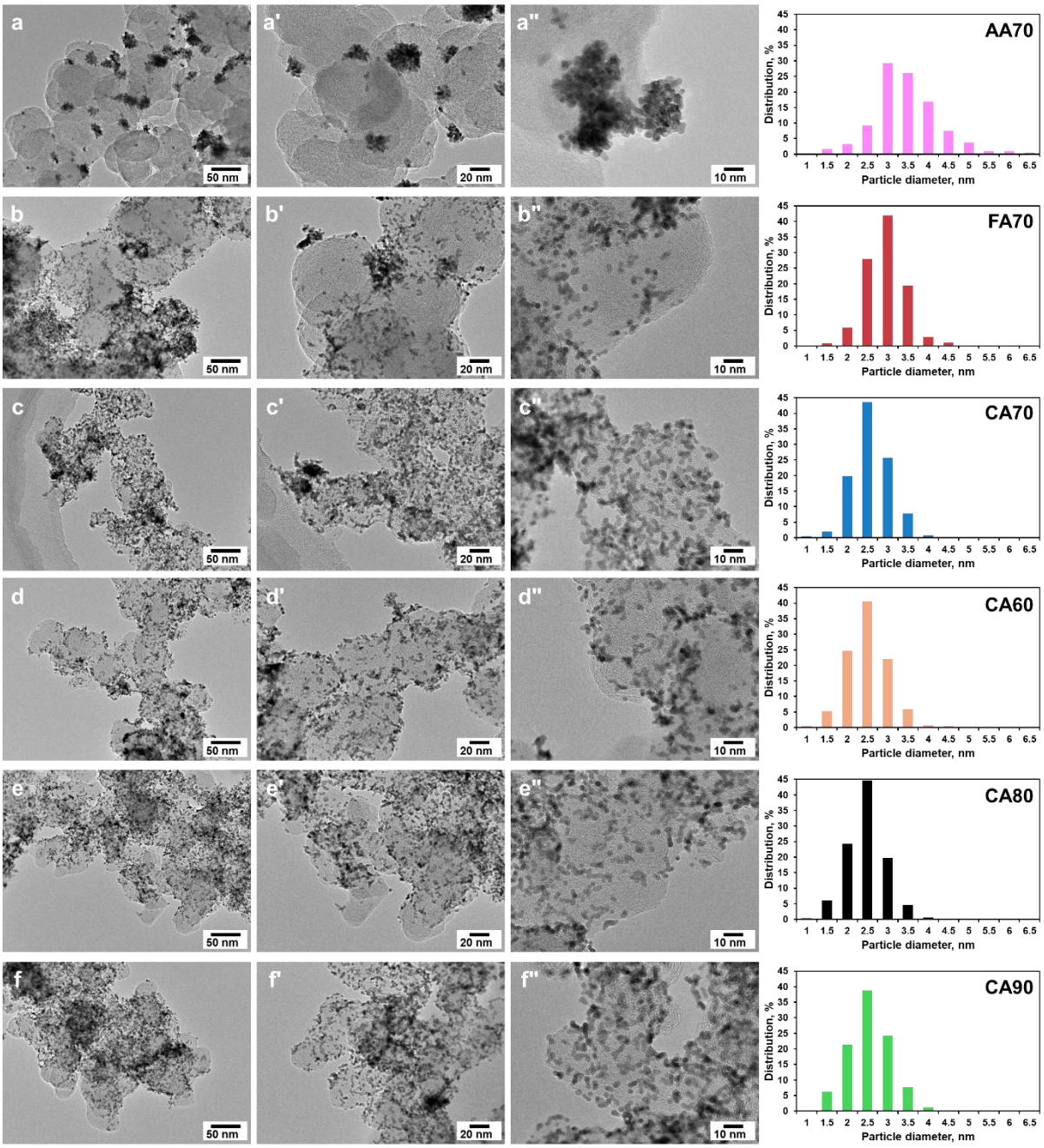

Figure 6. *TEM micrographs of the Pt/C catalysts synthesized in the carbon suspensions under different conditions: ascorbic acid (a, a', a"), formic acid (b, b', b"), citric acid at 70 °C (c, c', c"), citric acid at 60 °C (d, d', d"), citric acid at 80 °C (e, e', e"), citric acid at 90 °C (f, f', f") and histograms of the NPs size distribution in the corresponding catalysts*

The combination of these influencing factors is believed to largely determine the size of platinum NPs formed. It should be noted that a deeper interpretation of the differences in the NPs' size, their aggregation features, and the nature of their spatial (over the surface of the support) distribution in the "carboxylic acid" syntheses is hindered due to a lack of knowledge about the mechanisms of NPs nucleation/growth. In particular, there is a lack of information on the overlap or time separation between the nucleation and growth stages of new-phase nuclei, as well as on the nature of the interaction between the components of the reaction medium and the surface of the carbon support. Nevertheless, the differences established in the kinetics of the reduction reactions of platinum precursors to NPs provide important information, the accumulation of which would allow us not only to control the synthesis conditions but also to optimize them. Interestingly, it is the ascorbic

acid synthesis that has demonstrated significant differences both in the kinetics of the multistage transformation of Pt(IV) → Pt(0)x and in the structural and morphological characteristics of the resulting Pt/C material.

Electrochemical behaviour of the synthesized Pt/C catalysts

The deposited Pt/C materials are known to be among the best catalysts for hydrogen oxidation and oxygen reduction in hydrogen-air fuel cells with a proton-exchange membrane [41-43]. Their microstructure (shape, size, and spatial distribution of Pt NPs) has a significant impact on important functional parameters that determine the effectiveness of PEMFCs, such as ESA and ORR activity. Therefore, the materials obtained have been tested as the ORR catalysts. The electrochemical behaviour of the Pt/C materials has been studied using cyclic and linear-sweep voltammetry (Figures 7, S8, and S9). All the cyclic voltammograms (CVs) have a typical shape characteristic of Pt/C catalysts (Figure 7a, 7b and S9a). The current values in the CVs double-layer region are the same for all the samples, but differ in the hydrogen and oxygen regions, increasing in the order: AA70 << << FA70 < HiSPEC 4000 < CA60 ≤ CA70 ≈ CA80 ≤ CA90. The catalysts ESA values calculated from the CVs' hydrogen adsorption/desorption regions grow in the same order (Table 2).

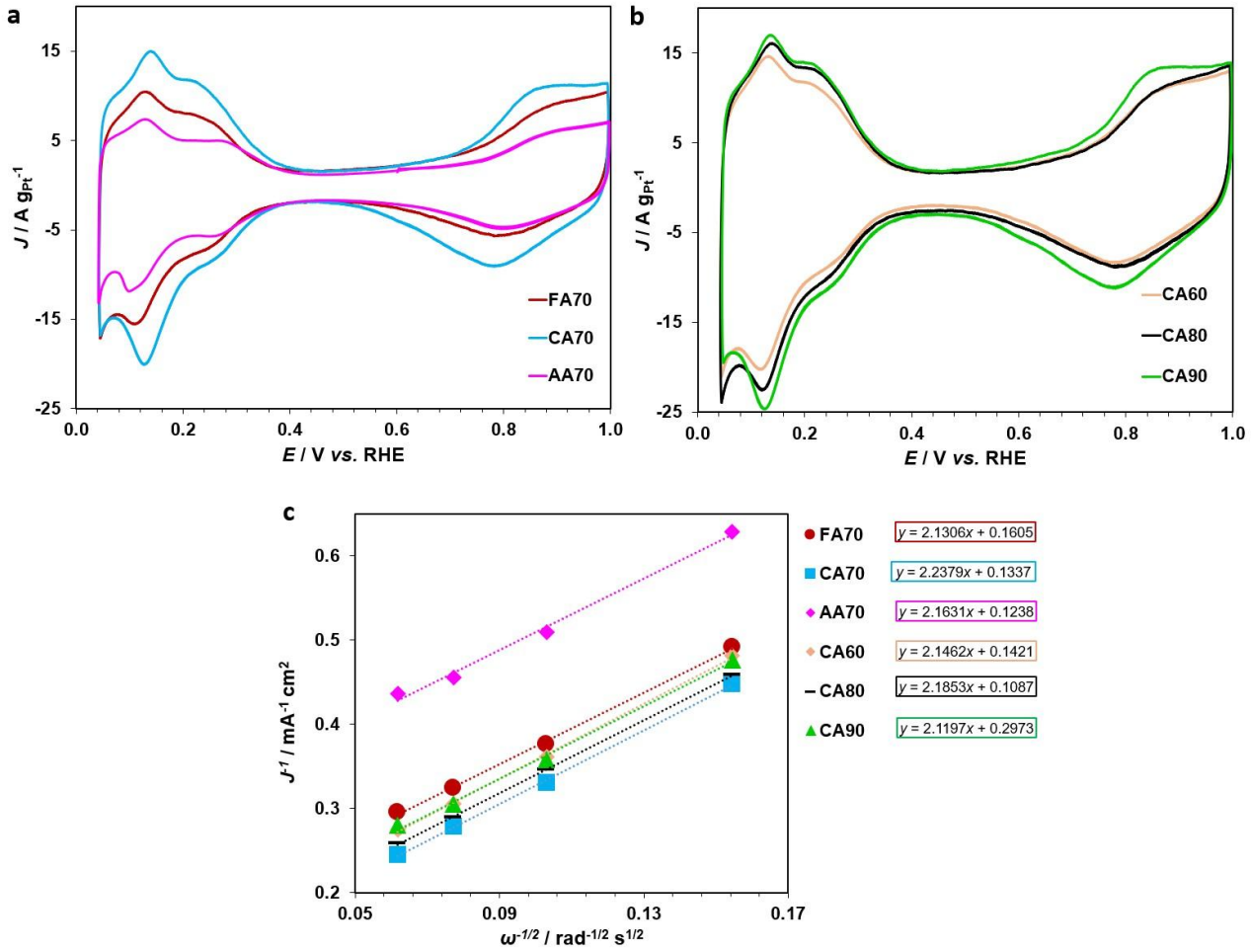

Figure 7. *(a,b) Cyclic voltammograms for the Pt/C samples, (c) J^{-1} - $\omega^{-1/2}$ dependencies (Koutecký -Levich coordinates) at 0.90 V. The potential sweep rate is 20 mV s^{-1}, 0.1 M $HClO_4$ solution saturated with Ar (a,b) and O_2 (c) at atmospheric pressure*

Thus, the samples synthesized by the citric acid method have the highest ESA value, while the product of ascorbic acid synthesis exhibits the lowest. This nature of the ESA change is due to the

catalyst microstructure features described earlier*, i.e.* platinum NPs have the smallest size in the CA series samples, while the AA70 material combines a larger NPs size and the formation of numerous nanoflower type aggregates.

The linear sweep voltammograms (LSVs) characterizing the ORR activity of the catalysts at different electrode rotation speeds are shown in Figures S8 and S9b, and the corresponding Koutecký-Levich plots are shown in Figure 7c. The catalyst's mass activity values in the ORR (Table 2) were calculated from kinetic currents determined by extrapolating the straight-line segments in the Koutecký-Levich coordinates to the J^{-1} axis (Figure 7c). Based on the slopes of these segments, the number of electrons involved in the electroreduction of one oxygen molecule has been determined (Table 2). It turns out to be close to 4 for all the catalysts. This means that the electroreduction of oxygen to water proceeds via a 4-electron mechanism. The values of the average specific activity of platinum, calculated from the mass activity to the ESA, have also turned out to be close for all synthesized catalysts (Table 2). Also, the averaged specific activity of the synthesized catalysts is higher than that of the commercial analog HiSPEC4000 (Table 2).

Table 2. *Parameters characterizing the Pt/C materials' electrochemical behaviour*

Sample	ESA / m^2 *per* g of Pt	$E_{1/2}$ / V	$I\ m^{-1}$ / A *per* g of Pt	J / A *per* m^2 of Pt (ESA)
AA70	32±3	0.884	192±19	6.0±1.2
FA70	45±5	0.905	356±40	7.9±1.6
CA70	65±7	0.915	468±47	7.2±1.4
CA60	60±6	0.911	434±43	7.2±1.4
CA80	66±7	0.913	419±42	6.4±1.3
CA90	69±7	0.909	417±42	6.0±1.2
HiSPEC4000	57±6	0.895	231±23	4.1±0.8

At the same time, the mass activity values, as well as the half-wave potentials, increase in approximately the same order, which correlates well with the catalyst ESA: AA70 < HiSPEC4000 < FA70 < CA90 ≈ CA80 ≤ CA60 ≤ CA70. The exception is the CA90 sample, whose ESA is the largest and whose mass activity is slightly lower than for CA60 and CA70. However, the accuracy in determining the corresponding parameters is ±10%, which eliminates the established differences. Therefore, the Pt/C catalysts synthesized by the citric acid method are superior not only to AA70 and FA70 samples in terms of the ESA and the ORR mass activity, but also to the well-known commercial catalyst with a 40 % platinum loading (HiSPEC4000) (Table 2 and [44]), which makes them promising for testing in PEMFC membrane electrode assemblies (MEAs).

Conclusions

This study presents a novel approach to investigating the kinetics of platinum nanoparticle and Pt/C electrocatalyst formation, based on in-situ monitoring of chemical transformations in real time during liquid-phase synthesis. The kinetics of the multistage reduction of $[PtCl_6]^{2-}$ were studied by combining RGB colorimetric measurements and open-circuit chronopotentiometry, which reflected changes in the redox potential of the reaction medium.

For each synthesis method (each reducing agent), we have obtained reproducible dependencies of colour intensity and potential on time, with characteristic areas corresponding to specific stages of transformation and associated with the chemical mechanism of the process. In particular, we have reliably recorded the moment of platinum NP formation in solution and approximated the induction period preceding nucleation of metallic platinum, the duration of nucleation, and the total transformation time. The possibility of reliably identifying these characteristic transformation stages

has been confirmed by analysing UV-vis absorption spectra of dilute solutions obtained by sampling the reaction medium during synthesis. Taking into account the relationships between the characteristic sections of the ClrInt - t and E - t dependences established for the solutions, we have studied the kinetics of platinum phase formation in carbon suspensions based on the corresponding solutions, according to the type of the *E* - *t* curves. This made it possible to identify the effect of the dispersed carbon support on transformation kinetics.

It was found that the ascorbic acid synthesis differs significantly from the formic acid and citric acid ones, both in its kinetics and in the characteristics of the Pt/C product formed. The duration of the induction period, the nucleation stage, and the total Pt(IV) → Pt(0)x transformation time decrease in the order FA70 > CA70 >> AA70. It has been found that the formation of platinum NPs in the ascorbic acid synthesis begins already during the transformation of Pt(IV) to Pt(II); this process starts after the transformation of Pt(IV) to Pt(II) for the other two reducing agents. The potential values at which the nucleation of platinum NPs begins (proceeds) in the studied solutions are in the range of about 100 mV and decrease in the order AA70 > FA70 > CA70. Synthesizing in the carbon suspensions rather than in solutions inhibits the transformation of platinum precursors into NPs during citric acid synthesis, which may be due to sorption of part of the reducing agent by the support, thereby decreasing its concentration in solution. At the same time, the transformations chemical mechanism does not seem to change. In the ascorbic acid synthesis, the introduction of dispersed carbon into the reaction medium significantly accelerates phase formation, which may be due to a noticeable contribution of heterogeneous (on the surface of the support) nucleation of NPs.

The increase in the temperature of the citric acid synthesis in the range of 60 to 90 °C has been established to accelerate the transformation and the duration of its separate stages (steps), but does not significantly affect the type of the ClrInt - *t* and *E* - *t* dependences, as well as the structural and morphological characteristics of the Pt/C materials formed.

All Pt/C materials obtained contain about 40 wt.% Pt loading. The size of platinum crystallites and NPs therein decreases in the order AA70 > FA70 ≥ CA70 ≈ CA60 ≈ CA80 ≈ CA90. At the same time, the AA70 sample is characterized by a strong non-uniformity of the NPs spatial distribution due to the formation of numerous aggregates in the form of nanoflowers.

The results of the study have shown that the electrochemical behaviour of the obtained Pt/C electrocatalysts correlates well with their structural and morphological characteristics. The AA70 electrocatalyst has demonstrated the lowest ESA and ORR mass activity values, the electrocatalysts synthesized by the citric acid method exhibiting the highest characteristics, *i.e*. the ESA values of 60 to 69 m^2 *per* g of Pt and the specific current values of 420 to 470 mA *per* g of Pt, which exceed equivalent characteristics of the HiSPEC4000 (Johnson Matthey) commercial analog.

The information capacity and simplicity of RGB colorimetry, combined with OCP monitoring, create a promising foundation for future technological innovations. With the present state of knowledge, not all characteristic features of the ClrInt - *t* and *E* - *t* dependencies cannot yet be interpreted unambiguously. The accumulation of experimental data using the proposed approach to study the kinetics of liquid-phase synthesis reactions, in combination with additional methods for analysing the composition of the reaction medium at various stages of transformation, will continue. In combination with other research methods, this may enable a comprehensive analysis of the ongoing transformations, reveal general patterns, and provide a deeper understanding of the specifics of each reaction.

Thus, the developed approach, which enables real-time monitoring of platinum compound transformations during synthesis, opens new possibilities for creating next-generation high-

performance electrocatalysts with improved characteristics. This is crucial for advancing hydrogen-air fuel cells and clean energy technologies.

Supplementary material

Additional data are available at https://pub.iapchem.org/ojs/index.php/JESE/article/view/3224, or from the corresponding author on request.

Acknowledgements: *This research was funded by the Strategic Academic Leadership Program of the Southern Federal University (Priority 2030). The authors are grateful to Maltsev, A.V. for the support in translation and editing processes. The authors are grateful to the Shared Use Center "High-Resolution Transmission Electron Microscopy" (SFedU, Rostov-on-Don) for conducting the TEM studies.*

References

[1] X. Wang, X. Chen, *Novel Nanomaterials for Biomedical, Environmental and Energy Applications*, Elsevier, Amsterdam, Netherlands, 2019. https://dx.doi.org/10.1016/C2017-0-01068-6

[2] P. Bhol, M. B. Bhavya, S. Swain, M. Saxena, A. K. Samal, Modern Chemical Routes for the Controlled Synthesis of Anisotropic Bimetallic Nanostructures and Their Application in Catalysis, *Frontiers in Chemistry* **8** (2020) 521371. https://dx.doi.org/10.3389/fchem.2020.00357

[3] S. Iravani, Surfactant-Free Synthesis of Metal and Metal Oxide Nanomaterials: A Perspective, *RSC Sustainability* **1** (2023) 72-82. https://dx.doi.org/10.1039/D2SU00088A

[4] J. Quinson, K. M. Ø. Jensen, From Platinum Atoms in Molecules to Colloidal Nanoparticles: A Review on Reduction, Nucleation and Growth Mechanisms, *Advances in Colloid and Interface Science* **286** (2020) 102300. https://dx.doi.org/10.1016/j.cis.2020.102300

[5] T. Yao, S. Liu, Z. Sun, Y. Li, S. He, H. Cheng, Y. Xie, Q. Liu, Y. Jiang, Z. Wu et al., Probing Nucleation Pathways for Morphological Manipulation of Platinum Nanocrystals, *Journal of the American Chemical Society* **134** (2012) 9410-9416. https://dx.doi.org/10.1021/ja302642x

[6] A. Rao, S. Roy, V. Jain, P. P. Pillai, Nanoparticle Self-Assembly: From Design Principles to Complex Matter to Functional Materials, *ACS Applied Materials & Interfaces* **15** (2023) 25248-25274. https://dx.doi.org/10.1021/acsami.2c05378

[7] T. S. Rodrigues, M. Zhao, T. H. Yang, K. D. Gilroy, A. G. M. da Silva, P. H. C. Camargo, Y. Xia, Synthesis of Colloidal Metal Nanocrystals: A Comprehensive Review on the Reductants, *Chemistry - A European Journal* **24** (2018) 16944-16963. https://dx.doi.org/10.1002/chem.201802194

[8] J. Quinson, S. Kunz, M. Arenz, Surfactant-Free Colloidal Syntheses of Precious Metal Nanoparticles for Improved Catalysts, *ACS Catalysis* **13** (2023) 4903-4937. https://dx.doi.org/10.1021/acscatal.2c05998

[9] J. Quinson, Colloidal Surfactant-Free Syntheses of Precious Metal Nanoparticles for Electrocatalysis, *Current Opinion in Electrochemistry* **34** (2022) 100977. https://dx.doi.org/10.1016/j.coelec.2022.100977

[10] D. Zhang, B. Gökce, S. Barcikowski, Laser Synthesis and Processing of Colloids: Fundamentals and Applications, *Chemical Reviews* **117** (2017) 3990-4103. https://dx.doi.org/10.1021/acs.chemrev.6b00468

[11] D. Gebauer, J. D. Gale, H. Cölfen, Crystal Nucleation and Growth of Inorganic Ionic Materials from Aqueous Solution: Selected Recent Developments, and Implications, *Small* **18** (2022) 2107735. https://dx.doi.org/10.1002/smll.202107735

[12] E. D. Bøjesen, B. B. Iversen, The Chemistry of Nucleation, *Crystal Engineering Communications* **18** (2016) 8332-8353. https://dx.doi.org/10.1039/c6ce01489e

[13] W. Dachraoui, T. R. Henninen, D. Keller, R. Erni, Multi-Step Atomic Mechanism of Platinum Nanocrystals Nucleation and Growth Revealed by In-Situ Liquid Cell STEM, *Scientific Reports* **11** (2021) 23965. https://dx.doi.org/10.1038/s41598-021-03455-w
[14] M. Harada, Y. Kamigaito, Nucleation and Aggregative Growth Process of Platinum Nanoparticles Studied by In Situ Quick XAFS Spectroscopy, *Langmuir* **28** (2012) 2415-2428. https://dx.doi.org/10.1021/la204031j
[15] M. V. Danilenko, V. E. Guterman, E. V. Vetrova, A. V. Metelitsa, K. O. Paperzh, I. V. Pankov, O. I. Safronenko, Nucleation/Growth of the Platinum Nanoparticles Under the Liquid Phase Synthesis, *Colloids and Surfaces A: Physicochemical and Engineering Aspects* **630** (2021) 127525. https://dx.doi.org/10.1016/j.colsurfa.2021.127525
[16] J. Quinson, M. Inaba, S. Neumann, A. A. Swane, J. Bucher, S. B. Simonsen, L. Theil Kuhn, J. J. K. Kirkensgaard, K. M. Jensen, M. Oezaslan, S. Kunz, M. Arenz, Investigating Particle Size Effects in Catalysis by Applying a Size-Controlled and Surfactant-Free Synthesis of Colloidal Nanoparticles in Alkaline Ethylene Glycol: Case Study of the Oxygen Reduction Reaction on Pt, *ACS Catalysis* **8** (2018) 6627-6635. https://dx.doi.org/10.1021/acscatal.8b00694
[17] V. Guterman, K. Paperzh, I. Novomlinskaya, I. Kantsypa, A. Khudoley, Y. Astravukh, I. Pankov, A. Nikulin, Advances in Liquid-Phase Synthesis: Monitoring of Kinetics for Platinum Nanoparticles Formation, and Pt/C Electrocatalysts with Monodispersive Nanoparticles for Oxygen Reduction, *Catalysts* **14** (2024) 728. https://dx.doi.org/10.3390/catal14100728
[18] C. Fyfe, S. Yu, J. Zhang, M. Reid, RGB Color Correction and Gamut Limitations in Smartphone-Based Kinetic Analysis of Chemical Reactions, *Analytical and Bioanalytical Chemistry* **417** (2025) 5753-5770. https://dx.doi.org/10.1007/s00216-025-06021-9
[19] H. Yu, J. Yu, L. Li, Y. Zhang, S. Xin, X. Ni, Y. Sun, K. Song, Recent Progress of the Practical Applications of the Platinum Nanoparticle-Based Electrochemistry Biosensors, *Frontiers in Chemistry* **9** (2021) 677876. https://dx.doi.org/10.3389/fchem.2021.677876
[20] L. Wang, H. Wang, Y. Nemoto, Y. Yamauchi, Rapid and Efficient Synthesis of Platinum Nanodendrites with High Surface Area by Chemical Reduction with Formic Acid, *Chemistry of Materials* **22** (2010) 2835-2841. https://dx.doi.org/10.1021/cm9038889
[21] U. S. Mehrotra, M. C. Agrawal, S. P. Mushran, Reduction of Hexachloroplatinate by Ascorbic Acid, *Journal of Inorganic and Nuclear Chemistry* **32** (1970) 2325-2329. https://dx.doi.org/10.1016/0022-1902(70)80514-0
[22] M. Luty-Błocho, A. Szot, V. Hessel, K. Fitzner, The Kinetics of the Redox Reaction of Platinum(IV) Ions with Ascorbic Acid in the Presence of Oxygen, *Materials* **16** (2023) 4630. https://dx.doi.org/10.3390/ma16134630
[23] C. S. Lin, M. R. Khan, S. D. Lin, The Preparation of Pt Nanoparticles by Methanol and Citrate, *Journal of Colloid and Interface Science* **299** (2006) 678-685. https://dx.doi.org/10.1016/j.jcis.2006.03.003
[24] R. Hirsch, *Exploring Colour Photography: A Complete Guide*, Laurence King Publishing, London (2005) p. 352. ISBN 1-85669-420-8.
[25] Z. Liu, X.Y. Ling, X. Su, J.Y. Lee, Carbon-supported Pt and PtRu nanoparticles as catalysts for a direct methanol fuel cell, *The Journal of Physical Chemistry B* **108** (2004) 8234-8240. https://doi.org/10.1021/jp049422b
[26] L. Vega, J. Garcia-Cardona, F. Viñes, P.L. Cabot, K.M. Neyman, Nanostructuring determines poisoning: tailoring CO adsorption on PtCu bimetallic nanoparticles, *Materials Advances* **3** (2022) 4159-4169. https://doi.org/10.1039/d2ma00196a
[27] J.I. Langford, A.J.C. Wilson, Scherrer after sixty years: A survey and some new results in the determination of crystallite size, *Journal of Applied Crystallography* **11** (1978) 102-113. https://doi.org/10.1107/S0021889878012844

[28] R. Sharma, S. Gyergyek, S.M. Andersen, Critical thinking on baseline corrections for electrochemical surface area (ECSA) determination of Pt/C through H-adsorption/H-desorption regions of a cyclic voltammogram, *Applied Catalysis B* **311** (2022) 121351. https://doi.org/10.1016/j.apcatb.2022.121351

[29] K. Shinozaki, J.W. Zack, R.M. Richards, B.S. Pivovar, S.S. Kocha, Oxygen reduction reaction measurements on platinum electrocatalysts utilizing rotating disk electrode technique, *Journal of The Electrochemical Society* **162** (2015) F1144-F1158. https://doi.org/10.1149/2.1071509jes

[30] S. Chen, Q. Yang, H. Wang, S. Zhang, J. Li, Y. Wang, W. Chu, Q. Ye, L. Song, Initial Reaction Mechanism of Platinum Nanoparticle in Methanol-Water System and the Anomalous Catalytic Effect of Water, *Nano Letters* **15** (2015) 5961-5968. https://dx.doi.org/10.1021/acs.nanolett.5b02098

[31] Y. Xia, Y. Xiong, B. Lim, S. E. Skrabalak, Shape-Controlled Synthesis of Metal Nanocrystals: Simple Chemistry Meets Complex Physics? *Angewandte Chemie International Edition* **48** (2009) 60-103. https://dx.doi.org/10.1002/anie.200802248

[32] E. Y. Feng, R. Zelaya, A. Holm, A. C. Yang, M. Cargnello, Investigation of the Optical Properties of Uniform Platinum, Palladium, and Nickel Nanocrystals Enables Direct Measurements of Their Concentrations in Solution, *Colloids and Surfaces A: Physicochemical and Engineering Aspects* **601** (2020) 125007. https://dx.doi.org/10.1016/j.colsurfa.2020.125007

[33] M. V. Danilenko, V. E. Guterman, I. N. Novomlinskiy, I. V. Pankov, The Effect of a Gas Atmosphere on the Formation of Colloidal Platinum Nanoparticles in Liquid Phase Synthesis, *Colloid and Polymer Science* **301** (2023) 433-443. https://dx.doi.org/10.1007/s00396-023-05077-2

[34] G. C. Halford, S. Hertle, H. N. Nambiar, M. L. Personick, Using Electrochemistry to Benchmark, Understand, and Develop Noble Metal Nanoparticle Syntheses, *ACS Nanoscience Au* **5(4)** (2025) 240-261. https://dx.doi.org/10.1021/acsnanoscienceau.5c00051

[35] S. E. Stanca, O. Vogt, G. Zieger, A. Ihring, J. Dellith, A. Undisz, M. Rettenmayr, H. Schmidt, Electrochemical Growth Mechanism of Nanoporous Platinum Layers, *Communications Chemistry* **4** (2021) 98. https://dx.doi.org/10.1038/s42004-021-00535-w

[36] S. T. Briskeby, M. Tsypkin, R. Tunold, S. Sunde, Preparation of Electrocatalysts by Reduction of Precursors with Sodium Citrate, *RSC Advances* **4** (2014) 44185-44192. https://dx.doi.org/10.1039/c4ra06639a

[37] T. Odoom-Wubah, Z. Li, Z. Lin, T. Tang, D. Sun, J. Huang, Q. Li, Ascorbic Acid Assisted Bio-Synthesis of Pd-Pt Nanoflowers with Enhanced Electrochemical Properties, *Electrochimica Acta* **228** (2017) 474-482 https://dx.doi.org/10.1016/j.electacta.2017.01.107

[38] I. I. Ponomarev, K. M. Skupov, O. M. Zhigalina, D. N. Khmelenin, E. S. Vtyurina, E. N. Cherkovskiy, V. G. Basu, A. D. Modestov, Deposition of Pt Nanoparticles by Ascorbic Acid on Composite Electrospun Polyacrylonitrile-Based Carbon Nanofiber for HT-PEM Fuel Cell Cathodes, *Catalysts* **12** (2022) 891. https://dx.doi.org/10.3390/catal12080891

[39] G. Zangari, Fundamentals of Electrodeposition, in Encyclopedia of Interfacial Chemistry: Surface Science and Electrochemistry, Elsevier, Amsterdam, 2018, pp. 141-160. https://dx.doi.org/10.1016/B978-0-12-409547-2.11700-7

[40] Q. L. Jiang, Z. D. Peng, X. F. Xie, K. Du, G. R. Hu, Y. X. Liu, Preparation of High Active Pt/C Cathode Electrocatalyst for Direct Methanol Fuel Cell by Citrate-Stabilized Method, *Transactions of Nonferrous Metals Society of China* **21** (2011) 127-132. https://dx.doi.org/10.1016/S1003-6326(11)60688-2

[41] A. Nyabadza, É. McCarthy, M. Makhesana, S. Heidarinassab, A. Plouze, M. Vazquez, D. Brabazon, A Review of Physical, Chemical and Biological Synthesis Methods of Bimetallic Nanoparticles and Applications in Sensing, Water Treatment, Biomedicine, Catalysis and

Hydrogen Storage, *Advances in Colloid and Interface Science* **321** (2023) 103010. https://dx.doi.org/10.1016/j.cis.2023.103010

[42] K. Mishra, N. Devi, S. S. Siwal, V. K. Thakur, Insight Perspective on the Synthesis and Morphological Role of the Noble and Non-Noble Metal-Based Electrocatalyst in Fuel Cell Application, *Applied Catalysis B: Environmental* **334** (2023) 122820. https://dx.doi.org/10.1016/j.apcatb.2023.122820

[43] D. Banham, S. Ye, Current Status and Future Development of Catalyst Materials and Catalyst Layers for Proton Exchange Membrane Fuel Cells: An Industrial Perspective, *ACS Energy Letters* **2** (2017) 629-638. https://dx.doi.org/10.1021/acsenergylett.6b00644

[44] Y. Lv, H. Liu, J. Li, J. Chen, Y. Song, A Convenient Protocol for the Evaluation of Commercial Pt/C Electrocatalysts toward Oxygen Reduction Reaction, *Journal of Electroanalytical Chemistry* **870** (2020) 114172. https://dx.doi.org/10.1016/j.jelechem.2020.114172